Cross-Coupling Compensation Using Gradient Ascent Method for Single-Transmitter Dual-Receiver Wireless Power Transfer

Ryo Matsumoto*, Toshiyuki Fujita†, Hiroshi Fujimoto‡
*Graduate School of Frontier Sciences, The University of Tokyo, Kashiwa, Japan
*matsumoto.ryo19@ae.k.u-tokyo.ac.jp, †t-fujita@edu.k.u-tokyo.ac.jp, ‡fujimoto@k.u-tokyo.ac.jp

***Abstract*—The coupling between the receiver coils *i.e.* cross-coupling is one of the main challenges in multiple receiver wireless power transfer. Previous studies showed that the cross-coupling can be compensated by adjusting the variable reactance in each receiver. However, the phase difference between the transmitter and receiver current is required in previous control methods, which is not a feasible approach in practical applications. This study proposes a control method for the variable reactances using the information of the input power. The proposed method compensates for the cross-coupling by tracking the maximum point of the input power with variable capacitors. The proposed control method is verified by experiment using pulsewidth modulation controlled switched capacitors.**

***Index Terms*—Multiple receiver, cross-coupling, switched capacitor, wireless power transfer (WPT).**

I. Introduction

Wireless power transfer (WPT) is an upcoming technology with the potential for various applications including electric vehicles [1], railway vehicles [2], consumer electronics [3], biomedical implants [4], and drones [5]. One of the attractive features of WPT is the ability to transfer power to multiple devices at the same time [6], [7]. For example, mobile phones, laptops, monitors, and desk lights can be simultaneously powered from a single transmitter (TX) coil installed beneath the table surface.

In multiple receiver WPT, the coupling between the receiver (RX) coils *i.e.* cross-coupling cannot be ignored when the devices are placed close to each other [8]. The cross-coupling causes the power to be transferred from one RX to another. This causes the received power of one RX to be affected by the position and load condition of other RXs. Previous studies [9], [10] showed that the influence of cross-coupling can be compensated by inserting optimal reactances in each RX. However, the control methods to achieve the optimal reactances are not discussed in [9], [10]. The authors of [11], [12] proposed control methods for variable capacitors adopted in each RX to compensate for the influence of cross-coupling. The phase difference between the TX and RX currents plays an important role in the control methods. However, this is not a feasible approach when considering practical constraints, as discussed in Section III-A.

This paper proposes a practical control method for variable capacitors to compensate for the cross-coupling in a single-TX dual-RX WPT system. The proposed method uses the information of the input power instead of the current phase to control the variable capacitors, thus providing a feasible solution for practical applications.

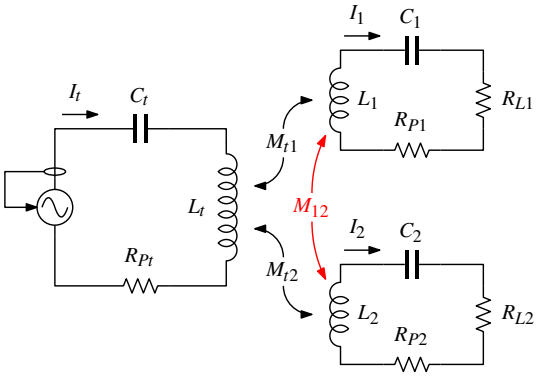

Fig. 1. Equivalent circuit of a two-receiver WPT system.

II. Principle of Cross-Coupling Cancellation

Fig. 1 shows the equivalent circuit of a WPT system consisting of a single TX and two RXs. L and C with subscripts t, 1 and 2 represent the self-inductances and compensation capacitances of the TX, RX1, and RX2. I_t, I_1, and I_2 represent the currents of the TX, RX1, and RX2. M_{t1}, M_{t2}, and M_{12} represent the mutual inductances between the TX and RX1, TX and RX2, and RX1 and RX2. R_{L1} and R_{L2} represent the load resistances of RX1 and RX2. R_{Pt}, R_{P1}, and R_{P2} represent the parasitic resistances of the TX, RX1, and RX2.

The circuit equations of RX1 and RX2 can be expressed as follows:

$$j\omega M_{t1} I_t + j\omega M_{12} I_2 = \left(j\omega L_1 + \frac{1}{j\omega C_1} + R_{L1} + R_{P1} \right) I_1, \tag{1}$$

$$j\omega M_{t2} I_t + j\omega M_{12} I_1 = \left(j\omega L_2 + \frac{1}{j\omega C_2} + R_{L2} + R_{P2} \right) I_2 \tag{2}$$

where ω is the operating angular frequency of the inverter. The total reactances of L_1 and C_1 in series, and L_2 and C_2 in series are defined as follows:

$$X_1 := \omega L_1 - \frac{1}{\omega C_1}, \quad X_2 := \omega L_2 - \frac{1}{\omega C_2}. \tag{3}$$

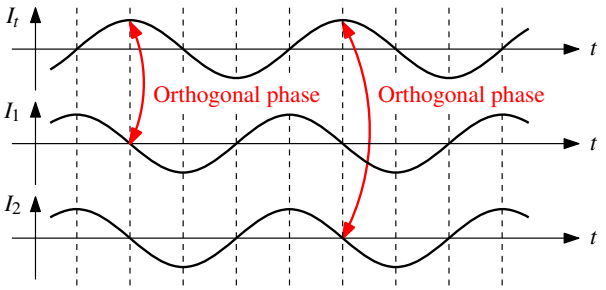

Fig. 2. Current waveforms when the cross-coupling is perfectly compensated.

Also, the total resistances of R_{L1} and R_{P1} in series, and R_{L2} and R_{P2} in series are defined as follows:

$$R_1 := R_{L1} + R_{P1}, \quad R_2 := R_{L1} + R_{P1}. \tag{4}$$

X_1 and X_2 can be adjusted by adopting variable capacitors in each RX and changing the values of C_1 and C_2. The influence of cross-coupling can be eliminated by canceling out the electromotive force (EMF) induced by the cross-coupling with X_1 and X_2 [10]. This condition can be described as:

$$j\omega M_{12} I_2 = jX_1 I_1, \quad j\omega M_{12} I_1 = jX_2 I_2. \tag{5}$$

From (1)–(5), the optimal values of X_1 and X_2 can be derived as follows:

$$X_{1opt} := \frac{\omega M_{12} I_2}{I_1} = \frac{\omega M_{12} M_{t2} R_1}{M_{t1} R_2}, \tag{6}$$

$$X_{2opt} := \frac{\omega M_{12} I_1}{I_2} = \frac{\omega M_{12} M_{t1} R_2}{M_{t2} R_1}. \tag{7}$$

In other words, the cross-coupling can be compensated by adjusting X_1 and X_2 to the values in (6) and (7). However, this is not a practical approach since the values of M_{t1}, M_{t2}, and M_{12} cannot be directly obtained if the RXs are placed in arbitrary positions.

III. Control Methods of Variable Reactance

A. Conventional Control Method

In order to control the reactances to the optimal values without the information of mutual inductances, the authors of [11], [12] proposed control methods using the information of the current phase. When the EMF induced by the cross-coupling is canceled out by X_1 and X_2, the circuit equations of RX1 and RX2 in Fig. 1 can be described as:

$$j\omega M_{t1} I_t = R_1 I_1, \quad j\omega M_{t2} I_t = R_2 I_2. \tag{8}$$

Equation (8) indicates that the phases of I_1 and I_2 lead the phase of I_t by 90° in the optimal condition, as shown in Fig. 2. In other words, the cross-coupling can be compensated by controlling $\angle I_1 - \angle I_t$ and $\angle I_2 - \angle I_t$ to 90° with the variable reactances. However, this approach entails the challenge of comparing the phase of high-frequency currents between physically separated circuits.

The authors of [11] proposed using wireless communication to send the information of the TX current phase to each RX.

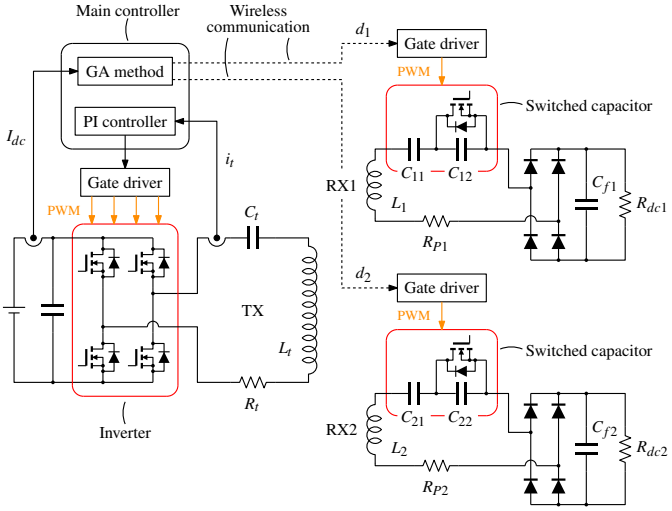

Fig. 3. Schematic of the proposed control method.

However, the practical implementation remains to be a technical issue, especially when considering the latency of wireless communication. The authors of [12] adopted additional circuits on the TX and each RX to obtain the TX current phase on the RX side. However, additional exclusive circuits increase the volume and cost of the system. Moreover, the manufacturing tolerance of circuit components can introduce errors in the phase information.

B. Proposed Control Method

In the following analysis, it is assumed that the amplitude of the TX current is regulated to a constant value I_{ref} as mentioned in [11], [12]. By solving (1)–(4), I_1 and I_2 can be expressed using X_1, X_2, and I_t as:

$$I_1 = \frac{-\omega M_{t1} X_2 - \omega^2 M_{t2} M_{12} + j\omega M_{t1} R_2}{\omega^2 M_{12}^2 - X_1 X_2 + R_1 R_2 + j(X_1 R_2 + X_2 R_1)} I_t, \tag{9}$$

$$I_2 = \frac{-\omega M_{t2} X_1 - \omega^2 M_{t1} M_{12} + j\omega M_{t2} R_1}{\omega^2 M_{12}^2 - X_1 X_2 + R_1 R_2 + j(X_1 R_2 + X_2 R_1)} I_t. \tag{10}$$

The input power of the TX can be expressed using I_1, I_2, and I_{ref} as:

$$P_{in}(X_1, X_2) = \frac{R_1}{2}|I_1|^2 + \frac{R_2}{2}|I_2|^2 + \frac{R_{Pt}}{2} I_{ref}^2. \tag{11}$$

From (8) and (11), the optimum input power when the cross-coupling is compensated can be expressed as:

$$P_{opt} = \left(\frac{\omega^2 M_{t1}^2}{2R_1} + \frac{\omega^2 M_{t2}^2}{2R_2} + \frac{R_{Pt}}{2} \right) I_{ref}^2. \tag{12}$$

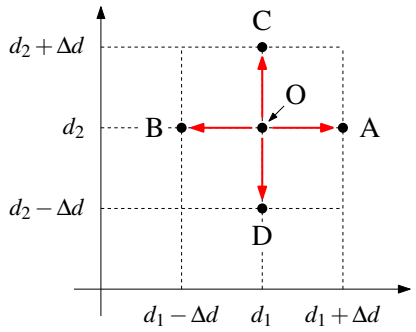

Fig. 4. Set of points used for the CFD approximation.

From (9)–(12), the difference between P_{opt} and P_{in} can be transformed to the following combination of squared terms:

$$\begin{aligned} &P_{opt} - P_{in}(X_1, X_2) \\ &= \left\{ \frac{1}{2R_1}(\omega M_{t1} R_2 X_1 - \omega^2 M_{12} M_{t2} R_1)^2 \right. \\ &+ \frac{1}{2R_2}(\omega M_{t2} R_1 X_2 - \omega^2 M_{12} M_{t1} R_2)^2 \\ &\left. + \left(\frac{\omega^2 M_{t1}^2}{2R_1} + \frac{\omega^2 M_{t2}^2}{2R_2} \right) (X_1 X_2 - \omega^2 M_{12}^2)^2 \right\} \frac{I_{ref}^2}{J^2 + K^2} \end{aligned} \tag{13}$$

where

$$\begin{aligned} J &= X_1 X_2 - \omega^2 M_{12}^2 - R_1 R_2, \\ K &= X_1 R_2 + X_2 R_1. \end{aligned}$$

Since R_1 and R_2 are positive values, the right-hand side of (13) is greater than or equal to zero. Therefore, the following inequality can be derived:

$$P_{in}(X_1, X_2) \leq P_{opt}. \tag{14}$$

The right-hand side of (13) is equal to zero only under the following condition:

$$X_1 = \frac{\omega M_{12} M_{t2} R_1}{M_{t1} R_2}, \quad X_2 = \frac{\omega M_{12} M_{t1} R_2}{M_{t2} R_1}. \tag{15}$$

These values are equivalent to the optimal values of X_1 and X_2 when the cross-coupling is compensated, as shown in (6), (7). From the above analysis, it can be concluded that P_{in} reaches its maximum value only when the cross-coupling is compensated by X_1 and X_2.

Based on the above discussion, the following approach to compensate for the cross-coupling without using the information of the current phase can be derived. In fact, the cross-coupling can be compensated by searching the values of X_1 and X_2 which maximize P_{in}. Fig. 3 shows the schematic of the proposed control method. The amplitude of I_t is regulated to a constant value by modulating the pulse width of the inverter with a PI controller. Pulsewidth modulation (PWM) controlled switched capacitors [13], [14] are adopted on each RX to realize variable reactances. Since the dc link voltage of the TX is constant, P_{in} is proportional to I_{dc}. Therefore, a gradient ascent (GA) method [15] is adopted to search the duty cycles of the switched capacitors d_1 and d_2 which maximize I_{dc}. The mathematical form of I_{dc} as a function of d_1 and d_2 cannot be obtained explicitly, since the circuit parameters such as M_{t1}, M_{t2}, and M_{12} are unknown in practical scenarios. Therefore, a central finite difference (CFD) approximation is applied to use the GA method in this paper. The gradient of I_{dc} can be approximated by:

$$\nabla f(d_1, d_2) = \begin{bmatrix} \dfrac{f(d_1 + \Delta d, d_2) - f(d_1 - \Delta d, d_2)}{2\Delta d} \\ \dfrac{f(d_1, d_2 + \Delta d) - f(d_1, d_2 - \Delta d)}{2\Delta d} \end{bmatrix} \tag{16}$$

where $f(d_1, d_2)$ denotes the mathematical form of I_{dc} as a function of d_1 and d_2. Δd denotes the sampling radius of the CFD approximation. d_1 and d_2 are updated iteratively based on the following equation:

$$\begin{bmatrix} d_1 \\ d_2 \end{bmatrix} \leftarrow \begin{bmatrix} d_1 \\ d_2 \end{bmatrix} + \alpha \nabla f(d_1, d_2) \tag{17}$$

where α denotes the learning rate of the GA method. The GA method is performed by using the set of points shown in Fig. 4 and executing the following five steps at constant intervals.

1) Move to point A.
2) Measure I_{dc} at point A and move to point B.
3) Measure I_{dc} at point B and move to point C.
4) Measure I_{dc} at point C and move to point D.
5) Measure I_{dc} at point D and calculate the gradient at point O based on (16). If the gradient is smaller than a pre-determined threshold, stop the procedure. If not, update the coordinate of point O based on (17) and return to step 1.

The execution interval of each step is designed sufficiently longer than the settling time of the transient response of the circuit. It should be noted that this method requires sending the values of d_1 and d_2 to each RX via wireless communication. However, since d_1 and d_2 are scalars, they are less sensitive to communication delays when compared to the phase information of I_t, I_1, and I_2.

IV. Experiment

An experimental prototype of the proposed system is developed to verify the proposed method, as shown in Fig. 5. The specifications of the experimental setup are listed in Table I. The first RX coil is placed $65\,\mathrm{mm}$ above the TX coil, and the second RX coil is placed $20\,\mathrm{mm}$ above the first RX coil. The second RX coil is horizontally aligned with the TX coil, while the center of the first RX coil is misaligned from the TX coil by $55\,\mathrm{mm}$. The switched capacitors are designed such that the equivalent capacitances can be controlled from $55\,\mathrm{nF}$ to $92\,\mathrm{nF}$. The PI controller and the GA method are implemented on a digital signal processing board.

Fig. 6 shows the input power and the phase difference between I_t, I_1, and I_2 measured at steady state when manually changing the duty cycles of the switched capacitors between

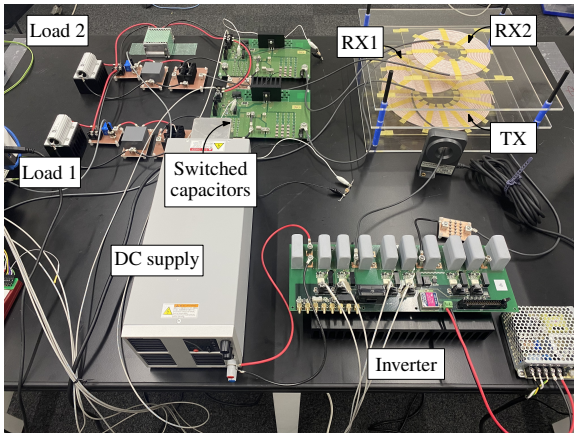

Fig. 5. Experimental setup.

TABLE I
SPECIFICATIONS OF EXPERIMENTAL SETUP.

Description	Symbol	Value
Operating frequency	-	100 kHz
Input DC voltage	V_{dc}	50.0 V
Reference of TX current amplitude	I_{ref}	4.0 A
Self-inductance of TX	L_t	105.5 µH
Self-inductance of RX1	L_1	29.9 µH
Self-inductance of RX2	L_2	29.5 µH
Load resistance of RX1	R_{dc1}	5.0 Ω
Load resistance of RX2	R_{dc2}	5.0 Ω
Mutual inductance of TX and RX1	M_{t1}	8.4 µH
Mutual inductance of TX and RX2	M_{t2}	8.4 µH
Mutual inductance of RX1 and RX2	M_{12}	−7.7 µH
Series connected capacitors of RX1	C_{11} C_{12}	91.7 nF 133.9 nF
Series connected capacitors of RX2	C_{21} C_{22}	91.8 nF 133.8 nF
Sampling radius of the CFD approximation	Δd	0.025
Execution interval of the GA method	-	100 ms
Learning rate of the GA method	α	0.02

0.35 and 0.65. The duty cycles are varied in increments of 0.05, resulting in 49 measurement points. The TX current amplitude is regulated to 4 A by the PI controller. By comparing Fig. 6(a) and Fig. 6(b), it can be seen that P_{in} is maximum and the phase differences between I_1 and I_t, I_2 and I_t are both 90° when d_1 and d_2 are slightly larger than 0.5. This result shows good agreement with the analysis in Section III-B and validates that the maximum point of P_{in} coincides with the cross-coupling compensation point.

Fig. 7 shows the trajectories of the duty cycles of the switched capacitors when searching for the maximum power point with the GA method. The initial values of d_1 and d_2 are set to 0.72. The final values of d_1 and d_2 after the convergence of the GA method are 0.506 and 0.514, respectively. This result shows good agreement with the results in Fig. 6 and indicates that the maximum power point is successfully being tracked by the GA method. Fig. 8 shows the voltage and current waveforms of the resonant circuit after the convergence of the GA method. I_{1sw}, V_{1sw}, I_{2sw}, and V_{2sw} represent the drain current and drain-source voltage of the MOSFETs in

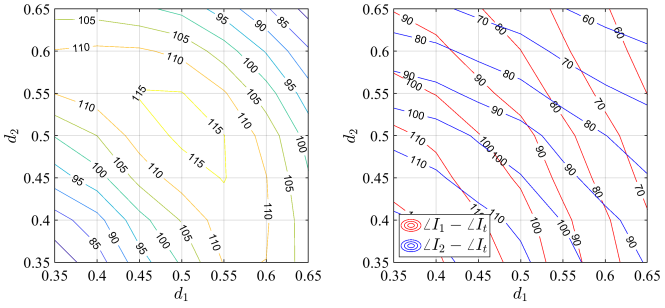

(a) (b)

Fig. 6. Experimental results of the (a) input power and (b) phase difference when manually changing the duty cycles of the switched capacitors.

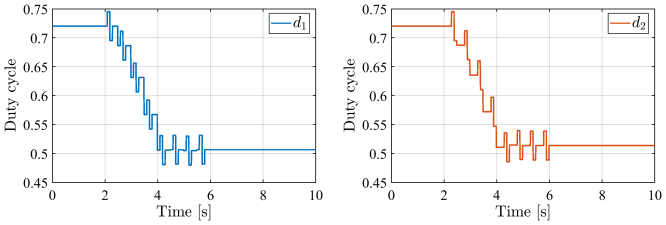

(a) (b)

Fig. 7. Trajectories of the duty cycles of the switched capacitors when applying the GA method.

the switched capacitors. The phase differences between the fundamental harmonics of I_t, I_1, and I_2 are $\angle I_1 - \angle I_t = 90.4°$ and $\angle I_2 - \angle I_t = 90.2°$, indicating that the cross-coupling is successfully compensated by the proposed method.

Fig. 9 and Table II show the comparison between the proposed method and three comparison cases. In the comparison cases, the resonance frequencies of RX1 and RX2 are tuned to the operating frequency *i.e.* 100 kHz using passive capacitors. In Case 1 and Case 2, the power is transferred exclusively to RX1 or RX2 by removing the other RX from the setup. In the proposed method and Case 3, the power is transferred simultaneously to RX1 and RX2. Case 1 and Case 2 are introduced to emulate the ideal power transfer characteristics to each RX when there is no cross-coupling. In all cases, the amplitude of I_t is regulated to 4 A by the PI controller. As

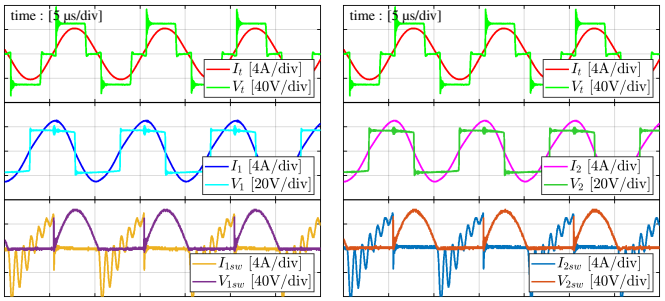

(a) (b)

Fig. 8. (a) Waveforms of TX and RX1 and (b) waveforms of TX and RX2 after the convergence of the GA method.

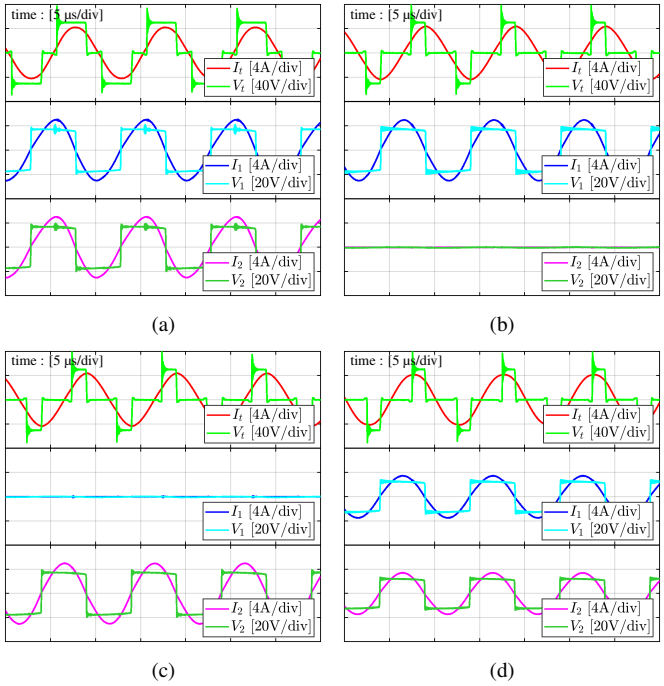

Fig. 9. Waveforms of TX, RX1, and RX2 of the proposed method and three comparison cases. (a) Case 1. (b) Case 2. (c) Case 3. (d) Case 4.

TABLE II
COMPARISON OF PHASE DIFFERENCE AND RECEIVED POWER

	$\angle I_1 - \angle I_t$	$\angle I_2 - \angle I_t$	P_1	P_2
Proposed	90.4°	90.2°	49.6 W	50.1 W
Case 1 RX1 only	89.7°	-	50.9 W	0 W
Case 2 RX2 only	-	91.4°	0 W	51.5 W
Case 3 RX1 and RX2	44.5°	45.5°	24.6 W	23.9 W

shown in Table II, the values of P_1 and P_2 in Case 1 and Case 2 show good agreement with those in the proposed method. On the other hand, the values of P_1 and P_2 in Case 3 decrease by 52% and 54% compared to those in Case 1 and Case 2 as a result of cross-coupling. In addition, $\angle I_1 - \angle I_t$ and $\angle I_2 - \angle I_t$ are far from 90° in Case 3. These results indicate that the ideal power transfer characteristics under zero cross-coupling can be achieved by the proposed method even under the presence of cross-coupling.

V. CONCLUSION

This paper proposed a practical control method for variable reactances to compensate for the cross-coupling in single-TX dual-RX WPT. Conventional methods relied on the information of the phase difference between the TX and RX currents to control the variable reactances. This paper revealed that the maximum point of the input power coincides with the cross-coupling compensation point in dual-RX WPT systems. The proposed method compensates for the cross-coupling by tracking the maximum point of the input power with the variable reactances. The experimental results showed that the ideal characteristics under zero cross-coupling can be achieved by the proposed method. The application of the proposed method to more than three RXs will be investigated in future studies.

ACKNOWLEDGEMENT

This work was partly supported by JST SPRING Grant Number JPMJSP2108.

REFERENCES

[1] A. N. Azad, A. Echols, V. A. Kulyukin, R. Zane, and Z. Pantic, "Analysis, optimization, and demonstration of a vehicular detection system intended for dynamic wireless charging applications," *IEEE Transactions on Transportation Electrification*, vol. 5, no. 1, pp. 147–161, 2019.

[2] E. Sato and K. Kondo, "Feasible power control method with a low sampling frequency for bidirectional wireless power transfer in battery-powered railway vehicle systems," *IEEJ Journal of Industry Applications*, vol. 12, no. 6, pp. 1078–1087, 2023.

[3] S. Hui and W. Ho, "A new generation of universal contactless battery charging platform for portable consumer electronic equipment," *IEEE Transactions on Power Electronics*, vol. 20, no. 3, pp. 620–627, 2005.

[4] P. Si, A. P. Hu, S. Malpas, and D. Budgett, "A frequency control method for regulating wireless power to implantable devices," *IEEE Transactions on Biomedical Circuits and Systems*, vol. 2, no. 1, pp. 22–29, 2008.

[5] T. Ohori, X. Li, H. Nakanishi, S. Ozawa, and W. Hijikata, "Wireless power transfer system for mobile robots with impedance matching by adjusting position of driver coil," *IEEJ Journal of Industry Applications*, vol. 12, no. 5, pp. 945–952, 2023.

[6] B. L. Cannon, J. F. Hoburg, D. D. Stancil, and S. C. Goldstein, "Magnetic resonant coupling as a potential means for wireless power transfer to multiple small receivers," *IEEE Transactions on Power Electronics*, vol. 24, no. 7, pp. 1819–1825, 2009.

[7] Y. Zhang, T. Lu, Z. Zhao, F. He, K. Chen, and L. Yuan, "Selective wireless power transfer to multiple loads using receivers of different resonant frequencies," *IEEE Transactions on Power Electronics*, vol. 30, no. 11, pp. 6001–6005, 2015.

[8] W. Zhong and S. Y. R. Hui, "Auxiliary circuits for power flow control in multifrequency wireless power transfer systems with multiple receivers," *IEEE Transactions on Power Electronics*, vol. 30, no. 10, pp. 5902–5910, 2015.

[9] Q.-T. Duong and M. Okada, "Analysis of reactance compensation for eliminating cross-coupling in multiple-receiver inductive power transfer," in *2017 11th European Conference on Antennas and Propagation (EUCAP)*, 2017, pp. 492–495.

[10] M. Fu, T. Zhang, X. Zhu, P. C.-K. Luk, and C. Ma, "Compensation of cross coupling in multiple-receiver wireless power transfer systems," *IEEE Transactions on Industrial Informatics*, vol. 12, no. 2, pp. 474–482, 2016.

[11] M. Ishihara, K. Fujiki, K. Umetani, and E. Hiraki, "Autonomous system concept of multiple-receiver inductive coupling wireless power transfer for output power stabilization against cross-interference among receivers and resonance frequency tolerance," *IEEE Transactions on Industry Applications*, vol. 57, no. 4, pp. 3898–3910, 2021.

[12] X. Xie, C. Xie, Y. Li, J. Wang, Y. Du, and L. Li, "Adaptive decoupling between receivers of multireceiver wireless power transfer system using variable switched capacitor," *IEEE Transactions on Transportation Electrification*, vol. 7, no. 4, pp. 2143–2155, 2021.

[13] F. Grazian, T. B. Soeiro, and P. Bauer, "Inductive power transfer based on variable compensation capacitance to achieve an ev charging profile with constant optimum load," *IEEE Journal of Emerging and Selected Topics in Power Electronics*, vol. 11, no. 1, pp. 1230–1244, 2023.

[14] R. Matsumoto, T. Fujita, and H. Fujimoto, "Communicationless reactance compensation using pwm-controlled switched capacitors for wireless power transfer," *IEEE Transactions on Power Electronics*, vol. 38, no. 10, pp. 13 194–13 206, 2023.

[15] C. Kim, Y. Gui, and C. C. Chung, "Maximum power point tracking of a wind power plant with predictive gradient ascent method," *IEEE Transactions on Sustainable Energy*, vol. 8, no. 2, pp. 685–694, 2017.